JOURNAL OF SOLID STATE CHEMISTRY **122,** 324–332 (1996)
ARTICLE NO. 0121

Copper–Zinc–Cobalt–Aluminium–Chromium Hydroxycarbonates and Mixed Oxides

Simone Morpurgo,[1] Mariano Lo Jacono, and Piero Porta

Centro del Consiglio Nazionale delle Ricerche su 'Struttura e Attività Catalitica di Sistemi di Ossidi' (SACSO), c/o Dipartimento di Chimica, Università La Sapienza, Piazzale Aldo Moro 5, 00185 Rome, Italy

Received August 7, 1995; in revised form November 21, 1995; accepted December 5, 1995

Hydroxycarbonate precursors with different Cu/Zn/Co/Al/Cr atomic ratios were prepared by coprecipitation of the metal nitrates with a stoichiometric amount of $NaHCO_3$ under controlled conditions of temperature, stirring, and pH. Cu–Zn–Co–Al–Cr mixed oxides were obtained by decomposition of the precursors at different temperatures (623, 723, and 973 K in air). The characterization has been performed by X-ray powder diffraction (XRPD), diffuse reflectance spectroscopy in the UV–VIS–NIR region (DRS), thermal analysis (TGA/DTA), BET surface area determination, and measurements of magnetic susceptibility. The XRPD patterns show that the precursors are quasi-amorphous layered double hydroxides (LDHs or hydrotalcite-like materials with the general stoichiometric formula: $M^{II}_6M^{III}_2(OH)_{16}CO_3 \cdot 4H_2O$, where M^{II} = Cu, Zn, Co and M^{III} = Al, Cr) containing a variable amount of $Cu_2(OH)_2CO_3$ (malachite). The thermal decomposition of the precursors occurred through complete dehydration of the sample (up to T = 573 K) and further release of CO_2 (up to T = 773 K). The decomposition of $Cu_2(OH)_2CO_3$ occurred in a single step at about 653 K. The mixed oxides obtained by calcination of the precursors at 623 K were poorly crystalline materials. Crystalline oxide mixtures containing CuO, ZnO, and spinels as $ZnCr_2O_4$, $ZnCo_2O_4$, $ZnAl_2O_4$, and Co_3O_4 in a solid solution were formed only at 973 K, after complete release of CO_2.

INTRODUCTION

Copper-based mixed oxides systems schematically represented as $Cu/ZnO/M_2O_3$ (M = Al, Cr, Ga) are widely known as industrial catalysts for the production of methanol, higher alcohols, and hydrocarbons through syngas reaction. A sort of synergic effect between the different components of the mixed oxides allows the catalytic activity to take place in relatively mild conditions ($T < 573$ K, $P \simeq 50$–100 atm) (1–8).

It has been shown that the presence of cobalt and chromium in some $Cu/ZnO/M_2O_3$-like catalysts results in a better selectivity toward the formation of higher alcohols and hydrocarbons with respect to methanol (9–13). Some authors (13, 14), however, have found that low cobalt contents are detrimental to the catalytic activity and, in general, it is not yet clear what is the cobalt-containing phase which really affects the catalyst selectivity.

The present work, which follows those on the Cu–Zn–Co–Al and Cu–Zn–Co–Cr systems (15, 16), is aimed at the synthesis and characterization of well interdispersed Cu–Zn–Co–Al–Cr mixed oxides obtained by thermal treatment of hydroxycarbonate precursors. The precursors have been prepared by coprecipitation, in the attempt of including all the metal cations in the same layered double hydroxide (LDH or hydrotalcite-like) structure (17, 18) having the stoichiometric formula $M^{II}_6M^{III}_2(OH)_{16}CO_3 \cdot 4H_2O$, where M^{II} = Cu, Zn, Co and M^{III} = Al, Cr. In order to obtain hydrotalcite-type compounds the M^{II}/M^{III} ratio has been kept about equal to three in each sample. The Cu/Zn ratio is also constant and close to 2.3. The cobalt content, which is added at the expense of copper and zinc, ranges from 0 to 15 at %, in steps of five. The main purpose of the study is to establish how the presence of cobalt affects the structural properties of the system.

EXPERIMENTAL

Preparation

The hydroxycarbonate precursors have been prepared by coprecipitation, i.e., placing a solution of the metal nitrates into a solution of $NaHCO_3$ at a constant temperature of 313 K and under vigorous stirring. The amount of $NaHCO_3$ employed was stoichiometric with respect to the coprecipitation reaction. The slurry was aged for 2 h. The pH after precipitation was ca. 6.5 and it was adjusted by dropwise addition of a NaOH solution until the final value was ca. 8. The color of the slurry was blue-green. The precipitate was repeatedly washed with distilled water, in order to eliminate the excess of Na^+ and NO_3^- ions, and dried under vacuum at room temperature for 4–5 days ($CaCl_2$ employed as a dehydratant). The dry product was

[1] To whom correspondence should be addressed.

0022-4596/96 $18.00

TABLE 1

Analytical Metal % Composition (Nominal % in Brackets), Phases Detected by XRPD in the Precursors and in the Oxides Calcined at 973 K, Surface Areas (ϕ) of the Samples Calcined at 723 and 973 K, Phase Composition (wt %) of the Oxides Calcined at 973 K, Phase Composition (Molar %) of the Spinels, Observed (a_o) and Calculated (a_c) Lattice Parameter, Curie Constant (C), and Weiss Temperature (Θ) Determined from the $1/\chi_A(Cr^{3+})$ vs T Plots

Samples	Co = 0		Co = 5		Co = 10		Co = 15	
Cu	54.9	(52.5)	51.1	(49.0)	47.7	(45.5)	45.5	(42.0)
Zn	20.5	(22.5)	19.6	(21.0)	18.7	(19.5)	17.4	(18.0)
Co	—	—	4.8	(5.0)	10.0	(10.0)	15.0	(15.0)
Al	11.5	(12.5)	11.3	(12.5)	11.1	(12.5)	11.3	(12.5)
Cr	13.0	(12.5)	13.2	(12.5)	12.5	(12.5)	10.8	(12.5)
XRPD precursors[a]	Hy+M		Hy+M		Hy+M		Hy+M	
XRPD oxides[a]	T, Z, S		T, Z, S		T, Z, S		T, S	
ϕ/m^2g^{-1}(723 K)	82.3		89.2		93.0		91.4	
ϕ/m^2g^{-1}(973 K)	18.1		16.6		18.1		17.6	
Oxide phase composition (wt%)								
CuO	57.4		53.2		49.5		47.1	
ZnO	8.8		5.3		2.0		0.0	
Spinel	33.8		41.5		48.5		52.9	
Spinel phase composition (mol%)								
$ZnCr_2O_4$	53.1		45.0		37.2		29.7	
$ZnAl_2O_4$	46.9		38.6		33.0		31.1	
$ZnCo_2O_4$	—		16.4		29.8		34.9	
Co_3O_4	—		—		—		4.3	
a_o(Å)	8.221		8.194		8.175		8.159	
a_c(Å)	8.213		8.195		8.178		8.152	
C	1.42		1.63		1.74		1.97	
Θ (K)	80.7		65.1		52.1		42.5	

[a] Symbols: Hy = hydrotalcite, M = malachite, T = tenorite, Z = zincite, S = spinel.

finely ground in an agate mortar. The content of residual Na^+ was analyzed by atomic absorption and found to be less than 0.05% in weight. The color of the compounds was blue-green. Note that the major problem connected to the precursor synthesis was the complementary formation of variable amounts of $Cu_2(OH)_2CO_3$ (malachite) as a by-product. In this respect, the effect of some experimental parameters (pH, T, digestion time, amount of $NaHCO_3$ employed for precipitation) has already been discussed in previous papers (15, 16). As a whole, the above synthesis conditions have been chosen in order to obtain, as far as possile, malachite-free LDH-type precursors.

The oxide products have been obtained by calcination of the corresponding precursors for 6 h at different temperatures (623, 723, and 973 K).

Methods

The characterization of both precursors and mixed oxides has been performed with the aid of several techniques such as atomic absorption for elemental analysis, X-ray powder diffraction (XRPD), thermogravimetric and differential thermal analysis (TG-DTA), UV–VIS–NIR diffuse reflectance spectroscopy (DRS), determination of the surface areas (BET method, N_2 as adsorbate), and measurements of magnetic susceptibility (Gouy method, in the temperature range 100–300 K). For more technical and instrumental details, see Refs. (15) and (16). Table 1 reports the analytical and nominal (in brackets) metal content for each sample.

RESULTS AND DISCUSSION

Precursors

The XRPD patterns of the precursors are reported in Fig. 1. They show the presence of a variable amount of crystalline $Cu_2(OH)_2CO_3$ (malachite) (19a), whose main peaks are superimposed to a quasi-amorphous structure. The content of crystalline malachite decreases at increasing cobalt content. The sample Co = 15 displays a pattern which, in spite of a very low crystallinity, resembles that typical of the hydrotalcite-like $Cu_2Zn_4Al_2(OH)_{16}CO_3 \cdot 4H_2O$ material (19b). This can especially be noticed in the

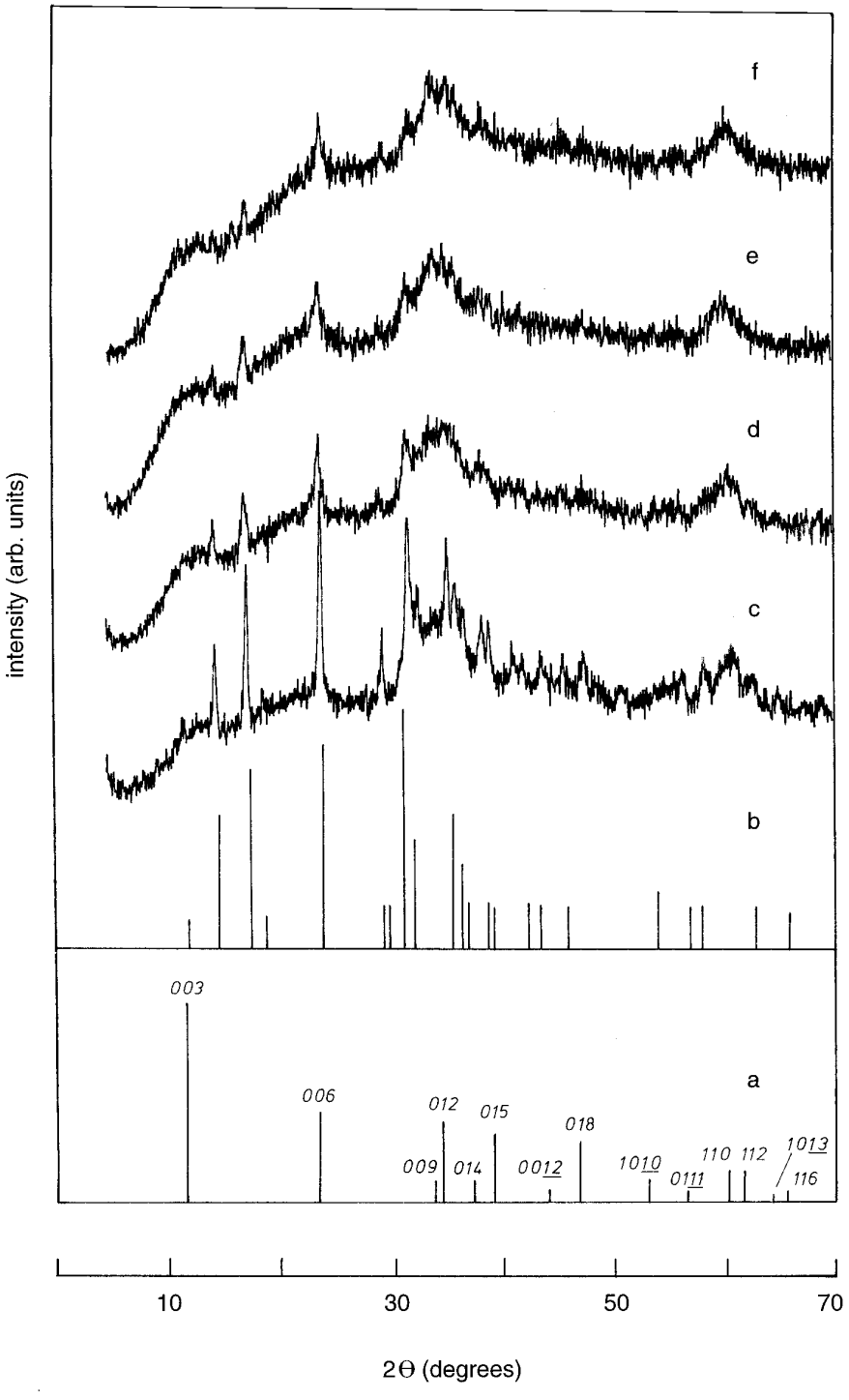

FIG. 1. XRPD patterns (Cu$K\alpha_1$ radiation) for Cu–Zn–Co–Al–Cr hydroxycarbonate precursors with different cobalt content: (c) Co = 0, (d) Co = 5, (e) Co = 10, and (f) Co = 15. At the bottom, the reference lines are given (a) for the hydrotalcite-like $Cu_2Zn_4Al_2(OH)_{16}CO_3 \cdot 4H_2O$ (19b) [with Miller (*hkl*) indices] and (b) for malachite, $Cu_2(OH)_2CO_3$ (19a).

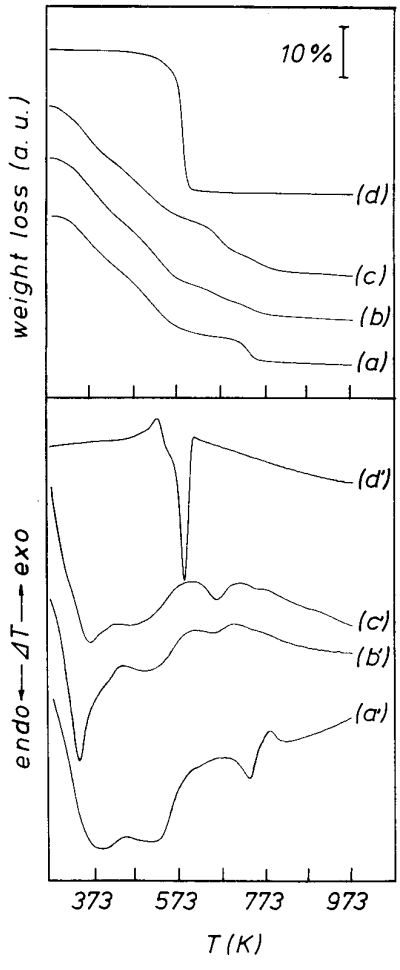

FIG. 2. Thermal analysis. Top: TGA for (a) $Cu_{4.2}Zn_{1.8}Cr_2(OH)_{16}CO_3 \cdot 4H_2O$ (16), (b) Co = 15, (c) Co = 0, and (d) $Cu_2(OH)_2CO_3$. Bottom: DTA for (a′) $Cu_{4.2}Zn_{1.8}Cr_2(OH)_{16}CO_3 \cdot 4H_2O$, (b′) Co = 15, (c′) Co = 0, and (d′) $Cu_2(OH)_2CO_3$.

2θ regions of the (003), (006), (009)–(015), and (110)–(112) reflections.

As already observed in a previous study (Cu–Zn–Co–Cr system) (16), the reflectance spectra of the hydroxycarbonate precursors (not shown) displayed the spectroscopic transitions of Cu^{2+} and Cr^{3+} in octahedral coordination (20–22). The transitions of octahedral Co^{2+} (23) were not evident, probably due to the simultaneous presence of Cu^{2+} and Cr^{3+}.

The thermogravimetric and differential thermal analysis (TGA-DTA) of the hydroxycarbonate precursors has been performed in air up to 973 K. The top and bottom diagrams of Fig. 2 show, respectively, the TGA and DTA curves of the samples Co = 0 and Co = 15 (as examples). For comparison the thermal patterns of malachite $[Cu_2(OH)_2CO_3]$ and of the hydrotalcite-type compound $[Cu_{4.2}Zn_{1.8}Cr_2(OH)_{16}CO_3 \cdot 4H_2O]$ (16) are reported. The sample with Co = 0 (whose XRPD pattern revealed, see Fig. 1, the presence of crystalline malachite plus an amorphous phase) shows, up to 623 K, thermal behavior which resembles that observed for the hydrotalcite-type material. The weight loss occurring up to about 573 K corresponds to a dehydration process which is the sum of the following steps: (i) dehydration of surface water, (ii) loss of crystallization water located between the positive layers of the structure, and (iii) dehydration of the OH groups. In the range of temperature where the CO_2 loss is expected to occur (16), two steps are visible: the first, in the range 643–683 K, is probably due to the release of CO_2 from the malachite structure (the relation can be particularly drawn from the DTA patterns) and the second, in the range 693–773 K, could correspond to the release of CO_2 from the amorphous hydrotalcite-type phase likely present in the mixture. The thermal behavior of the sample Co = 15 resembles, up to 573 K, that observed for the material with Co = 0, whereas from 573 to 773 K, a smoother decomposition occurs, most likely due to the loss of both residual water and CO_2 from the amorphous phase present in this sample (see Fig. 1).

Oxides

The XRPD patterns of the sample Co = 0, calcined for 6 h at different temperatures, are reported in Fig. 3. The dehydration process produces, for the sample calcined at 623 K, an amorphous material with only two weak peaks at $2\theta = 35.7°$ and 38.9° indicating the incipient segregation of tenorite (CuO) (19c). The XRPD pattern of the sample calcined at 723 K shows the formation of more crystalline CuO and of a spinel phase which may consist of $ZnAl_2O_4$ and $ZnCr_2O_4$ (19e, f), or their solid solution. At this temperature, the almost complete release of CO_2 allows the nucleation of detectable oxidic phases. The further calcination at 973 K results in the formation of highly crystalline CuO, ZnO (19d), and spinel. The cobalt-containing samples have shown a quite similar trend as a function of the calcination temperature.

The XRPD patterns of the samples having different cobalt content, calcined for 6 h at 973 K, are reported in Fig. 4. They generally reveal the formation of CuO, ZnO, and a spinel-like phase which, depending on the metal composition, may consist of $ZnAl_2O_4$, $ZnCr_2O_4$, $ZnCo_2O_4$, Co_3O_4, $CoAl_2O_4$, and $CoCr_2O_4$ (19e–l), very likely contained in a solid solution.

As the cobalt content increases, the following features result from a qualitative analysis of the X-ray diffraction patterns: (i) the relative peak intensity of CuO and ZnO decreases (no ZnO is detectable in the sample Co = 15), whereas the relative peak intensity of the spinel-like phase increases; (ii) the reflections corresponding to the spinel phase are progressively shifted to higher 2θ angles. Point (i) can be explained, as first, keeping into account that the

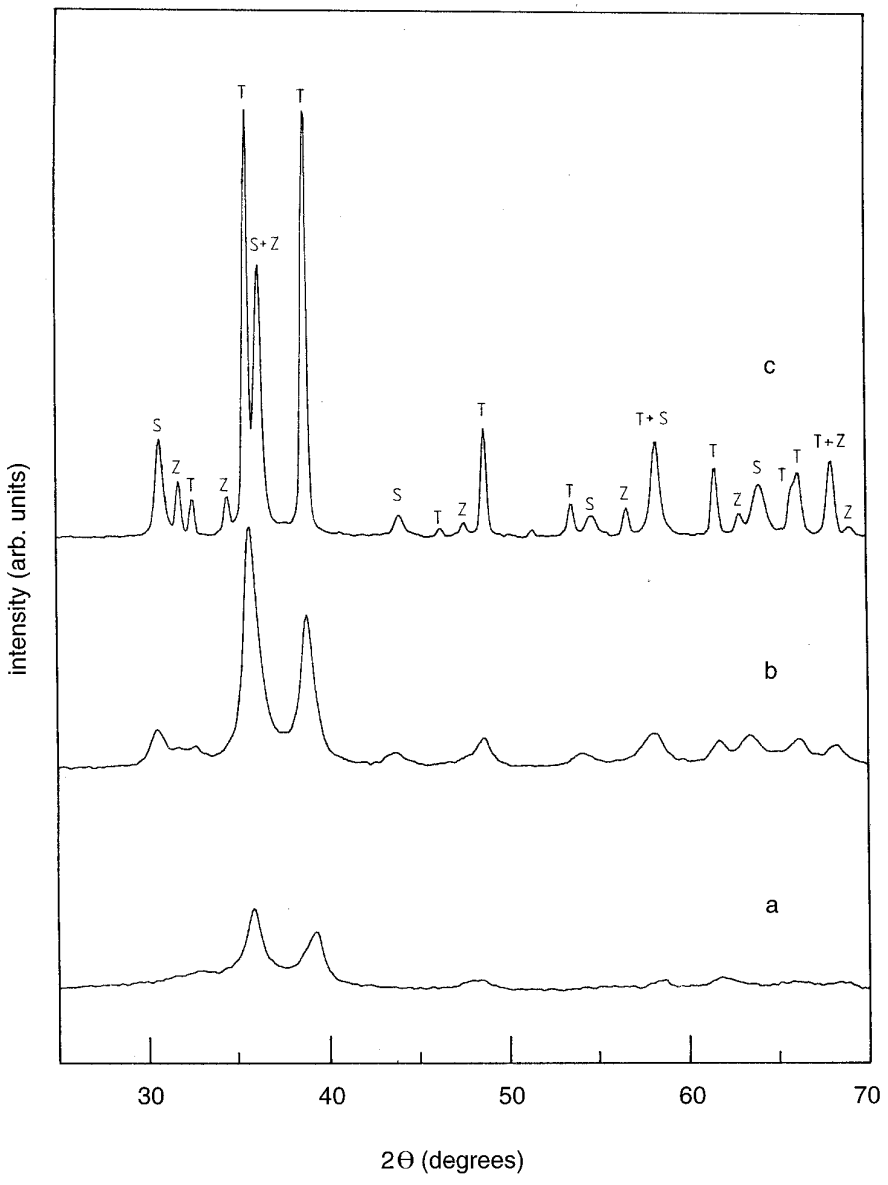

FIG. 3. XRPD patterns (Cu$K\alpha_1$ radiation) for the sample with Co = 0 calcined at different temperatures: (a) 623, (b) 723, and (c) 973 K. The phases observed at the final temperature (973 K) are indicated as T = tenorite, Z = zincite, and S = spinel.

total amount of copper and zinc in the samples decreases at increasing cobalt content. In addition, the decrease of ZnO and the subsequent intensity increase of the spinel reflections is due to the formation of $ZnCo_2O_4$. Point (ii) is related to the formation of a solid solution between the different spinels.

The samples calcined at 973 K were washed with a cold and dilute HCl solution in order to selectively remove CuO and ZnO and perform a more accurate XPRD characterization of the spinel phases. The XRPD patterns obtained for the washed materials are shown in Fig. 5. The observed lattice parameter, a_0, of the cubic spinels (reported in Table 1) was determined from the position of the X-ray reflections occurring up to $2\theta = 70°$.

Moreover, having considered the analytical composition of the samples and assumed a trial phase distribution for each spinel-like solid solution, the calculated values of the lattice parameters were derived according to the expression $a_c = \sum_i X_i a_i$, in which a_i is the value quoted in the literature for the ith pure phase contained in the spinel (a_i = 8.0848, 8.3275, 8.0946, 8.084 Å, respectively, for the end member $ZnAl_2O_4$ (19e), $ZnCr_2O_4$ (19f), $ZnCo_2O_4$ (19g), Co_3O_4 (19h) and X_i is the corresponding molar fraction. The a_c values, reported in Table 1 with the hypothe-

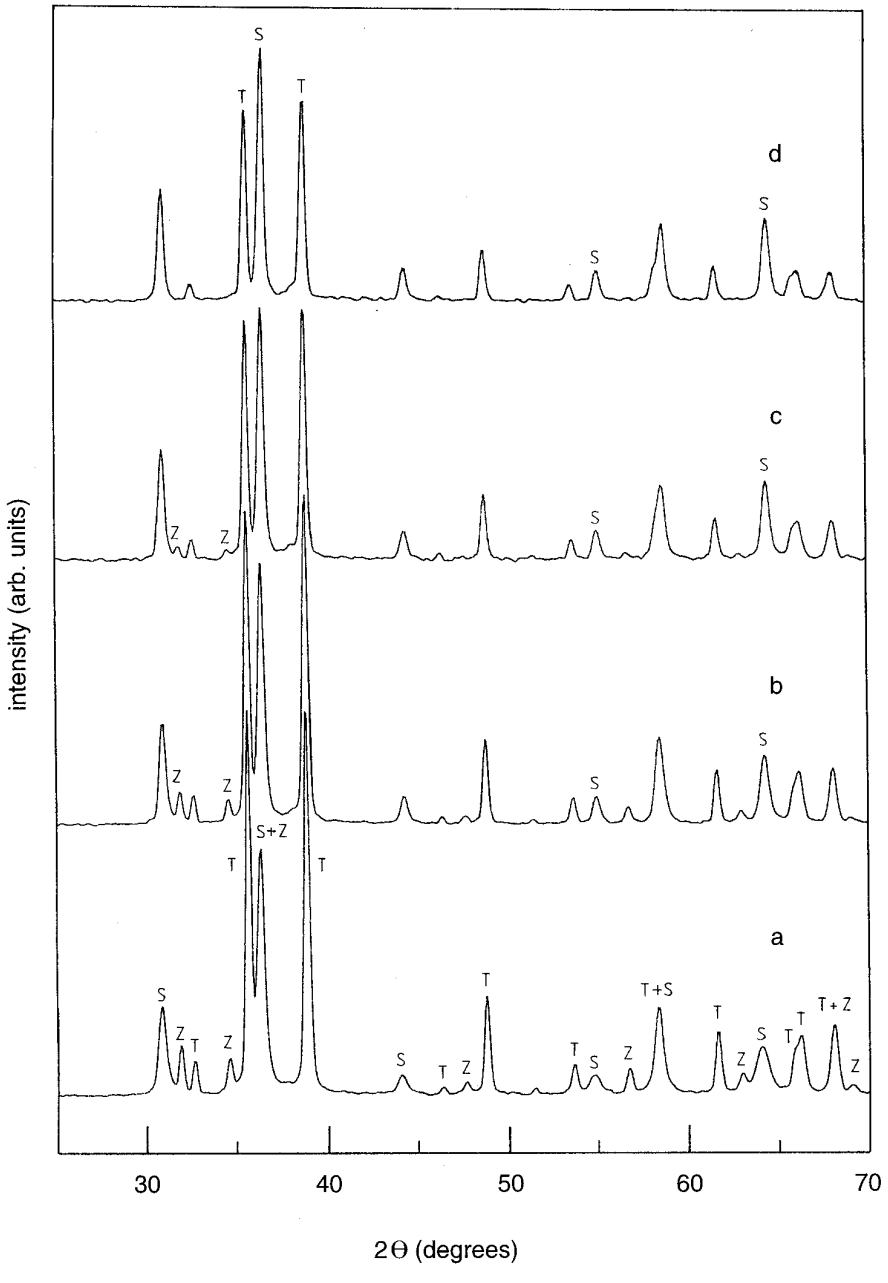

FIG. 4. XRPD patterns (Cu$K\alpha_1$ radiation) for the samples at different cobalt content calcined at 973 K: (a) Co = 0, (b) Co = 5, (c) Co = 10, and (d) Co = 15. The observed phases are indicated as T = tenorite, Z = zincite, and S = spinel.

sized phase distribution, are in good agreement with those observed. According to this result we can thus suggest that:

(i) for the sample Co = 0, the spinel phase is a Zn $[Cr_{2-y}Al_y]O_4$ solid solution (octahedral sites indicated in square brackets);

(ii) the addition of cobalt produces for the samples Co = 5 and Co = 10 the formation of a $Zn[Cr_{2-y-z}Al_y Co_z^{3+}]O_4$ solid solution, where Co^{3+} substitutes Cr^{3+} and Al^{3+} in the octahedral sites of the cubic spinel structure;

(iii) a $Zn_{1-x}Co_x^{2+}[Cr_{2-y-z}Al_yCo_z^{3+}]O_4$ spinel solid solution is formed for the sample Co = 15. In this mixed spinel Zn^{2+} and Co^{2+} ions are present in the tetrahedral sites of the structure as it occurs in pure $ZnAl_2O_4$, $ZnCr_2O_4$, $CoAl_2O_4$, and $CoCr_2O_4$ (19e, f, i, l).

The reflectance spectra of the samples with different cobalt content calcined for 6 h at 973 K (not shown) were dominated by the strong absorption threshold of CuO at ca. 12,500 cm^{-1} (24). The other relevant spectroscopic fea-

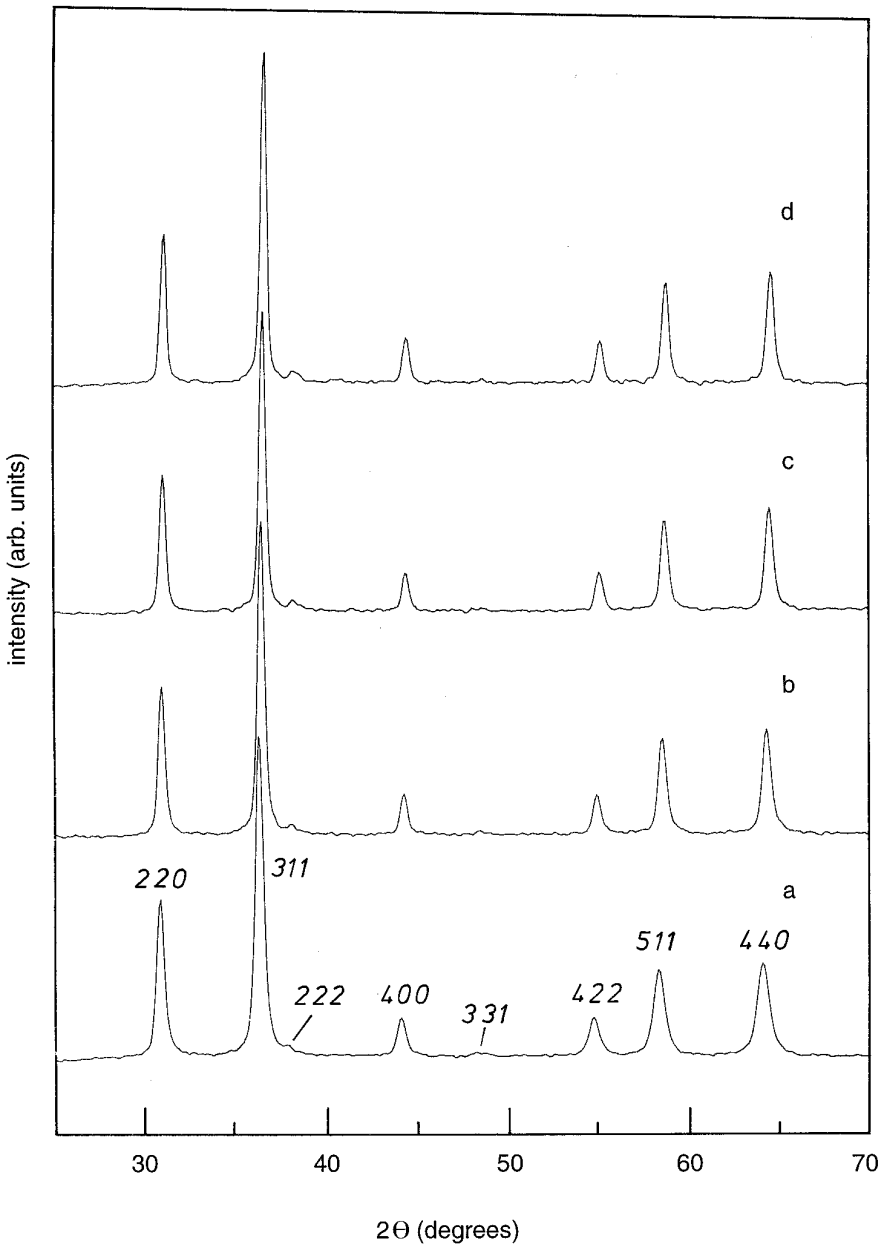

FIG. 5. XRPD patterns (Cu$K\alpha_1$ radiation) for the samples at different cobalt content, calcined at 973 K and washed with dilute HCl: (a) Co = 0, (b) Co = 5, (c) Co = 10, and (d) Co = 15. The Miller (*hkl*) indices are given for the spinel phase.

tures, related to the presence of the spinel phases, are better evidenced in the spectra of the corresponding samples treated with dilute HCl (Fig. 6), where the interference of CuO has been removed. The sample Co = 0 shows, in the near infrared region (4000–10,000 cm^{-1}), a broad band which cannot be ascribed to any *d–d* transition of the metals but, more likely, may be due to the presence of cationic vacancies in the spinel structure (25, 26). Two weak absorptions centred at 17,500 and 23,800 cm^{-1} correspond, in the same spectrum, to the first two spin-allowed $^4A_{2g} \rightarrow {}^4T_{2g}$ and $^4A_{2g} \rightarrow {}^4T_{1g}$ transitions of octahedral Cr^{3+} (22) (see for comparison the spectrum of the pure $ZnCr_2O_4$, reported at the bottom of the figure). In the cobalt-containing samples the following features become evident at the increase of the cobalt content: (i) the intensity and the width of the band observed in the near-infrared region tend to decrease and for the sample Co = 15 this band is replaced by a structured and narrower band centred at ca. 7000 cm^{-1}, undoubtedly associated with the $^4A_2 \rightarrow {}^4T_1(F)$ transition of tetrahedral Co^{2+} (20, 21); (ii) the two

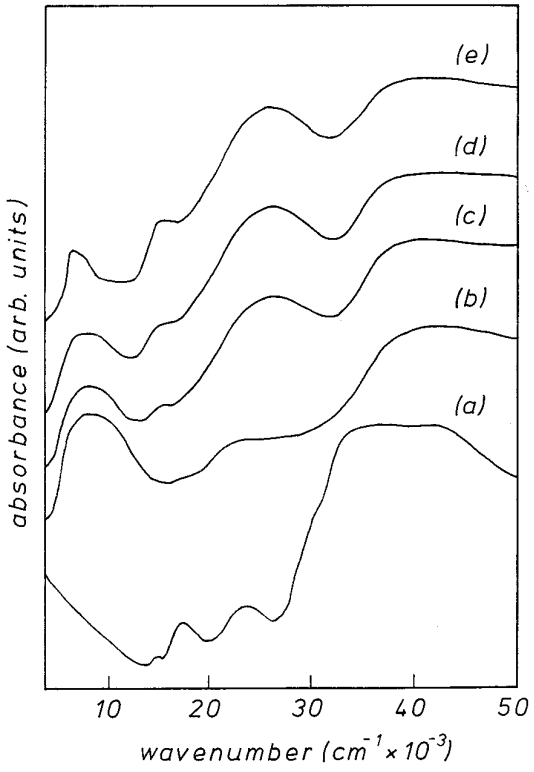

FIG. 6. Reflectance spectra for the samples at different cobalt content, calcined at 973 K and washed with dilute HCl: (b) Co = 0, (c) Co = 5, (d) Co = 10, and (e) Co = 15. Spectrum (a) is reference $ZnCr_2O_4$.

bands which, for the sample Co = 0, had been assigned to the transitions of octahedral Cr^{3+} no longer are distinguishable and are replaced by two different absorptions centred at 15,000 and 25,000 cm^{-1}. The former can either be assigned to tetrahedral $Co^{2+}[^4A_2 \rightarrow {}^4T_1(P)$ transition] or to octahedral Co^{3+} ($^1A_{2g} \rightarrow {}^1T_{2g}$ transition) (20, 21). The latter, because of the intensity, can be ascribed to the $Co^{2+} \rightarrow Co^{3+}$ charge transfer. The band observed for all samples at 34,000 cm^{-1} is probably due to $O^{2-} \rightarrow M^{3+}$ (M = Al, Co, Cr) charge transfer.

The magnetic susceptibility per gram (χ_{sp}) has been measured in the temperature range 100–300 K for the spinel-like solid solutions (HCl-treated samples) and for the reference compounds $ZnCr_2O_4$ and Co_3O_4 (both prepared in our laboratory from hydroxycarbonate precursors). Each χ_{sp} value has then been converted to the corresponding molar magnetic susceptibility, $\chi_M = \chi_{sp} \cdot M$ (M = molecular weight which, for the spinel solid solutions, has been derived from the phase composition reported in Table 1). The atomic susceptibility (χ_A) of Cr^{3+} in the spinel structure has finally been calculated subtracting from χ_M the correction for the diamagnetism (27) and, when present, the contribution of the atomic susceptibility of tetrahedral Co^{2+} which has been derived

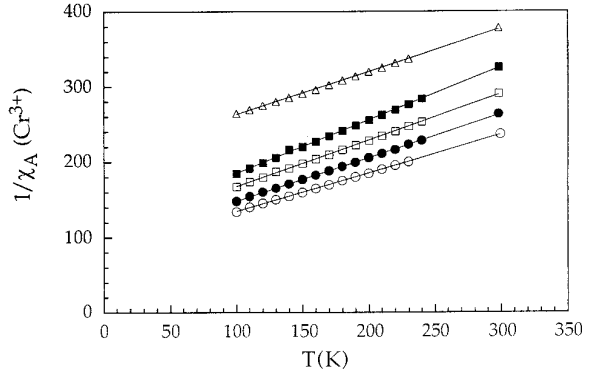

FIG. 7. $1/\chi_A(Cr^{3+})$ vs T plots for the samples at different cobalt content, calcined at 973 K and washed with dilute HCl (cubic spinels): (■) Co = 0, (□) Co = 5, (●) Co = 10, (○) Co = 15, and (△) reference $ZnCr_2O_4$.

from the measurement performed on pure Co_3O_4. The $1/\chi_A$ (Cr^{3+}) vs T plots so obtained for all samples and reference $ZnCr_2O_4$ are shown in Fig. 7. From this figure it is evident that, for the spinel solid solutions, χ_A (Cr^{3+}) is higher with respect to pure $ZnCr_2O_4$ and, moreover, it increases at increasing cobalt content. Having assumed for χ_A a Curie–Weiss temperature dependence ($\chi_A = C/T + \Theta$), the C and Θ values obtained from the plots have been reported in Fig. 8 as a function of the cobalt content in the octahedral sites of the spinel phases. Keeping into account that $ZnCr_2O_4$ is an antiferromagnetic spinel (28), the increase of C and the decrease of Θ (as far as Θ can be considered proportional to the extent of the antiferromagnetic interactions) at increasing cobalt content seem to indicate that the presence of

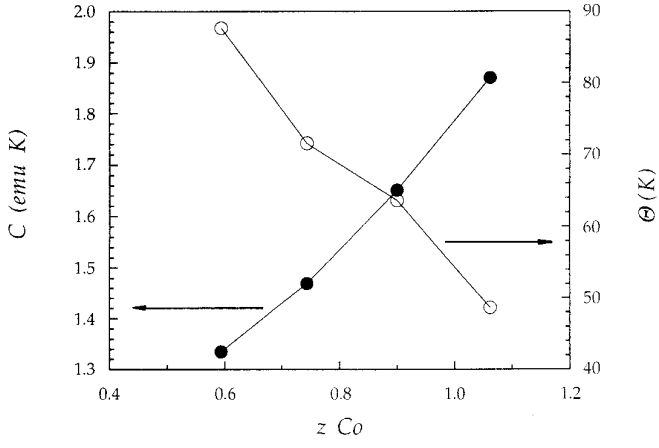

FIG. 8. Curie constant C (●) and Weiss temperature Θ (○) for the cubic spinel solid solutions $Zn[Cr_{2-y-z}Al_yCo_z^{3+}]O_4$ and $Zn_{1-x}Co_x^{2+}[Cr_{2-y-z}Al_yCo_z^{3+}]O_4$ (samples calcined at 973 K and washed with dilute HCl) vs Co^{3+} fraction z. At increasing z, respectively, Co = 0, 5, 10, and 15.

diamagnetic Co^{3+} contributes to the magnetic dilution of Cr^{3+}, causing a general increase of the corresponding atomic susceptibility. In a similar way, the higher values of $\chi_A(Cr^{3+})$ displayed by the mixed spinels with respect to $ZnCr_2O_4$ can be ascribed to the presence of diamagnetic Al^{3+} in octahedral coordination.

CONCLUSIONS

As a conclusion, we would like to stress the following points.

(i) Precursors are a mixture of a pseudo-amorphous hydrotalcite-type (LDH) phase and a variable amount of crystalline $Cu_2(OH)_2Co_3$ (malachite). The content of malachite decreases at increasing cobalt concentration.

(ii) The formation of malachite during the process of precipitation and digestion of the precursors depends, to some extent, on pH ($\geq$8.5), temperature ($\geq$323 K), prolonged digestion time of the precipitate, and excess of $NaHCO_3$ employed for precipitation.

(iii) Precursors display, as a whole, a thermal decomposition pattern resembling that of pure LDH compounds; however, the thermal decomposition of $Cu_2(OH)_2CO_3$ is also visible, especially for the Co = 0 sample.

(iv) The oxide products obtained by calcining the precursors at 973 K consist of a mixture of CuO, ZnO, and a $ZnCr_2O_4$–$ZnAl_2O_4$–$ZnCo_2O_4$–Co_3O_4 spinel solid solution. Cobalt is preferentially included as Co^{3+} in the octahedral sites of the spinel solid solution. At increasing cobalt content zinc is contained in the spinel solid solution rather than in ZnO.

(v) Presence of cationic vacancies is revealed by DR spectra in the spinels at low cobalt content. At increasing cobalt concentration the cationic vacancies tend to be filled by the inclusion of Co^{3+} in the octahedral and Co^{2+} in the tetrahedral sites.

(vi) The presence of diamagnetic Al^{3+} and Co^{3+} in the octahedral sites of the spinel structure decreases the antiferromagnetic interactions between the Cr^{3+} ions.

ACKNOWLEDGMENTS

We thank Dr. R. Dragone for technical assistance.

REFERENCES

1. G. Natta, *in* "Catalysis" (P. H. Emmet, Ed.), Vol. 3, Chap. 8. Reinhold, New York, 1955.
2. G. C. Chinchen, P. J. Denny, J. R. Jennings, M. S. Spencer, and K. C. Waugh, *Appl. Catal.* **36,** 1 (1988).
3. G. Ghiotti and F. Boccuzzi, *Catal. Rev.-Sci. Eng.* **29,** 151 (1987).
4. K. Klier, *Adv. Catal.* **31,** 243 (1982).
5. K. Klier, *Inorg. Chem.* **28,** 3868 (1989).
6. S. Metha, G. W. Simmons, K. Klier, and G. Hermann, *J. Catal.* **57,** 339 (1979).
7. C. Busetto, G. Del Piero, G. Manara, F. Trifirò, and A. Vaccari, *J. Catal.* **85,** 260 (1984).
8. G. Moretti, G. Fierro, M. Lo Jacono, and P. Porta, *Surf. Interface Anal.* **14,** 325 (1989).
9. W. M. H. Sachtler, *in* "Proceedings 8th International Congress on Catalysis, Berlin 1984." p. I–151. Verlag Chemie, Weinheim, 1984.
10. W. X. Pan, R. Cao, and G. L. Griffin, *J. Catal.* **114,** 447 (1988).
11. P. Courty, G. Durand, E. Freund, and A. Sugier, *J. Mol. Catal.* **17,** 241 (1982).
12. J. E. Baker, R. Burch, and S. E. Golunski, *Appl. Catal.* **53,** 279 (1989).
13. G. Fornasari, S. Gusi, F. Trifirò, and A. Vaccari, *Ind. Eng. Chem. Res.* **26,** 1501 (1987).
14. G. Fornasari, A. D'Huysser, L. Mintchev, F. Trifirò, and A. Vaccari, *J. Catal.* **135,** 386 (1992).
15. S. Morpurgo, M. Lo Jacono, and P. Porta, *J. Mater. Chem.* **4**(2), 197 (1994).
16. S. Morpurgo, M. Lo Jacono, and P. Porta, *J. Solid State Chem.* in press (1995).
17. W. Jones and M. Chibwe, *in* "Pillared Layered Structures" (I. V. Mitchell, Ed.), Chap. 2. Elsevier, London–New York, 1990.
18. M. A. Drezdon, *Inorg. Chem.* **27,** 4628 (1988).
19. X-Ray Powder Data File, ASTM-cards (a) 10-399 for malachite, $Cu_2(OH)_2CO_3$; (b) 38-487 for hydrotalcite-like $Cu_2Zn_4Al_2(OH)_{16}CO_3 \cdot 4H_2O$; (c) 5-661 for tenorite, CuO; (d) 36-1451 for zincite, ZnO; (e) 5-669 for $ZnAl_2O_4$; (f) 22-1107 for $ZnCr_2O_4$; (g) 23-1390 for $ZnCo_2O_4$; (h) 9-418 for Co_3O_4; (i) 10-458 for $CoAl_2O_4$; (l) 22-1084 for $CoCr_2O_4$.
20. A. B. P. Lever, *in* "Inorganic Electronic Spectroscopy." Elsevier, Amsterdam, 1984.
21. C. J. Ballhausen, *in* "Ligand Field Theory." McGraw Hill, New York, 1962.
22. R. A. Ford and O. F. Hill, *Spectrochim. Acta* **16,** 1318 (1960).
23. R. Pappalardo, D. L. Wood, and R. C. Linares, *J. Chem. Phys.* **35,** 2041 (1961).
24. O. V. Krylov, *in* "Catalysis by Non-metals," (E. M. Loebl, Ed.) p. 251 for CuO, p. 258 for ZnO. Academic Press, New York, 1970.
25. F. Trifirò and A. Vaccari, "Symposium on Structure-Activating Relationships in Heterogeneous Catalysis," p. 83. American Chemical Society, Boston, 1990.
26. R. A. Jackson, C. R. A. Catlow, and J. M. Thomas. *Catal. Lett.* **8,** 385 (1991).
27. P. W. Selwood, *in* "Magnetochemistry," 2nd ed., p. 78. Interscience, New York, 1964.
28. D. G. Wickham and J. B. Goodenough, *Phys. Rev.* **5,** 1156 (1959).